Earth, Planets and Space
a SpringerOpen Journal

FULL PAPER Open Access

Large-ion lithophile elements delivered by saline fluids to the sub-arc mantle

Tatsuhiko Kawamoto[1*], Kenji Mibe[2], Hélène Bureau[3], Solenn Reguer[4], Cristian Mocuta[4], Stefan Kubsky[4], Dominique Thiaudière[4], Shigeaki Ono[5] and Tetsu Kogiso[6]

Abstract

Geochemical signatures of arc basalts can be explained by addition of aqueous fluids, melts, and/or supercritical fluids from the subducting slab to the sub-arc mantle. Partitioning of large-ion lithophile elements between aqueous fluids and melts is crucial as these two liquid phases are present in the sub-arc pressure-temperature conditions. Using a micro-focused synchrotron X-ray beam, *in situ* X-ray fluorescence (XRF) spectra were obtained from aqueous fluids and haplogranite or jadeite melts at 0.3 to 1.3 GPa and 730°C to 830°C under varied concentrations of (Na, K)Cl (0 to 25 wt.%). Partition coefficients between the aqueous fluids and melts were calculated for Pb, Rb, and Sr ($D^{fluid/melt}_{Pb,\ Rb,\ Sr}$). There was a positive correlation between $D^{fluid/melt}_{Pb,\ Rb,\ Sr}$ values and pressure, as well as $D^{fluid/melt}_{Pb,\ Rb,\ Sr}$ values and salinity. As compared to the saline fluids with 25 wt.% (Na, K)Cl, the Cl-free aqueous fluids can only dissolve one tenth (Pb, Rb) to one fifth (Sr) of the amount of large-ion lithophile elements when they coexist with the melts. In the systems with 13 to 25 wt.% (Na, K)Cl, $D^{fluid/melt}_{Pb,\ Rb}$ values were greater than unity, which is indicative of the capacity of such highly saline fluids to effectively transfer Pb and Rb. Enrichment of large-ion lithophile elements such as Pb and Rb in arc basalts relative to mid-oceanic ridge basalts (MORB) has been attributed to mantle source fertilization by aqueous fluids from dehydrating oceanic plates. Such aqueous fluids are likely to contain Cl, although the amount remains to be quantified.

Keywords: Subduction zone magmatism; Mantle wedge; Water; H_2O; Brine; Trace element; Chlorine

Background

H_2O-rich fluids play significant roles in magma genesis and elemental recycling via subduction processes (Kushiro 1972; Green 1973; Perfit et al. 1980; Tatsumi and Eggins 1995; Keppler 1996; Bureau and Keppler 1999; Kawamoto 2006; Mibe et al. 2007; Kawamoto et al. 2012). The partitioning of large-ion lithophile elements such as Pb, Rb, and Sr between melts/crystals and aqueous fluids provides key information for estimating chemical features of slab-derived components because their abundances and isotopic compositions of Pb and Sr can distinguish subduction zone magmas from other types (Perfit et al. 1980; Tatsumi and Eggins 1995). In geochemical studies, three components are conventionally considered in the formation of arc basalts: the depleted mantle, an aqueous fluid-like component, and a melt-like component (Elliott et al. 1997; Pearce et al. 2005; Hanyu et al. 2012), the latter two being from downgoing slab materials. To understand arc basalt formation, it is important to assess the mixing ratios of slab-derived aqueous fluids and melts, and in order to do so, the partitioning of trace elements between melts and aqueous fluids must be determined.

Partitioning of many trace elements between aqueous fluids and melts or crystals can be determined by analyzing experimental products quenched from high-temperature and high-pressure (HTHP) conditions. While aqueous fluids dissolve silicate components under HTHP conditions (Anderson and Burnham 1965; Nakamura and Kushiro 1974), the solutes are not quenched into a single phase and can be recovered as a mixture of glass globules, quench crystals, and other materials (Schneider and Eggler 1986; Keppler 1994; Brenan et al. 1995). Such materials quenched from aqueous fluids under HTHP conditions can be analyzed after recovery through various methods including (1) leaching with water (Cullers et al. 1970; Flynn and Burnham 1978; Borchert et al. 2010a, b), (2) leaching with

* Correspondence: kawamoto@bep.vgs.kyoto-u.ac.jp
[1]Institute for Geothermal Sciences, Graduate School of Science, Kyoto University, Beppu 874-0903, Japan
Full list of author information is available at the end of the article

HCl acid (Keppler and Wyllie 1991; Keppler 1994, 1996; Bai and Koster van Groos 1999), (3) hand-picking (Schneider and Eggler 1986; Ayers and Eggler 1995; Brenan et al. 1995), (4) diamond aggregate trap followed by freezing (Kessel et al. 2005a), and (5) micro-PIXE (particle induced X-ray emission) analysis of samples quenched in a Bassett-type hydrothermal diamond anvil cell (HDAC; Figure 1A,B; Bassett et al. 1993; Bureau et al. 2003, 2005, 2007, 2010). Because of the differences in estimating fluid compositions, the reported values of partition coefficients between melts and aqueous fluids have varied to some extent (Ayers and Eggler 1995; Keppler 1996).

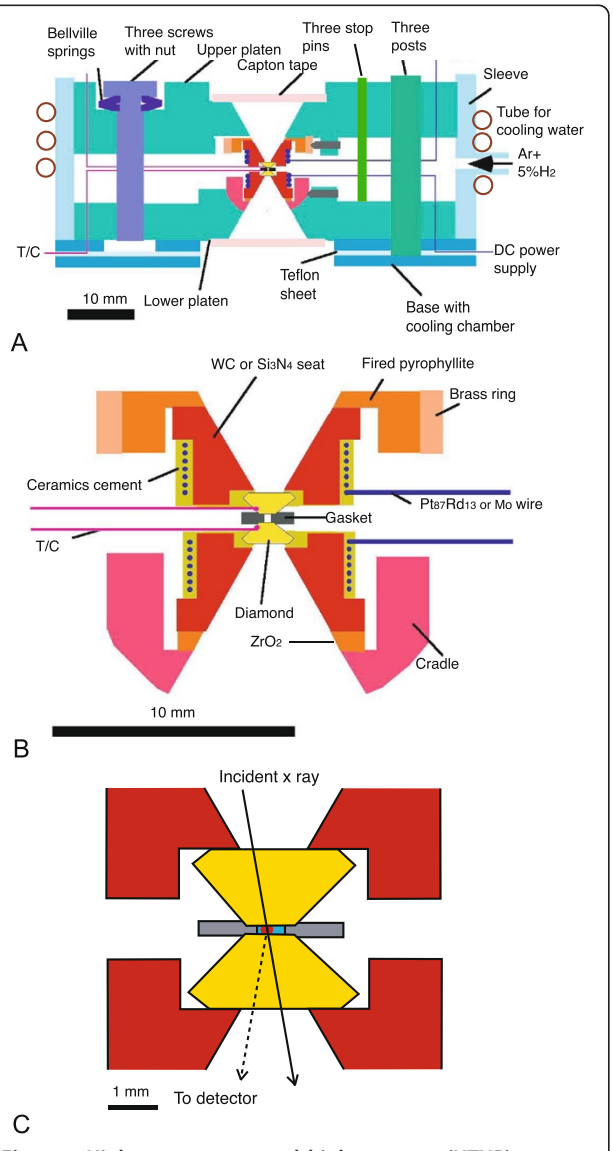

Figure 1 High-temperature and high-pressure (HTHP) experimental tool. (A) Illustration of a Bassett-type externally heated diamond anvil cell with some modifications. **(B)** Enlargement showing diamond anvils seated on WC or Si_3N_4 heating seats in the Bassett-type externally heated diamond anvil cell. A Y_2O_3-doped ZrO_2 ring was used as thermal insulator. **(C)** Geometry showing the 160° scattering angle between the incident X-ray and fluorescence detector, as used by Bureau et al. (2007) and in the present study. The large melt globule should be in contact with both surfaces of diamonds.

In order to obtain more reliable chemical compositions of aqueous fluids under HTHP conditions, *in situ* micro X-ray fluorescence (XRF) analysis was attempted using a Bassett-type HDAC in synchrotron facilities. *In situ* analyses of aqueous fluids have been carried out using Bassett-type HDACs either with normal diamond anvils (Sanchez-Valle et al. 2003; Bureau et al. 2005; Muñoz et al. 2005; Bureau et al. 2007, 2010) or with modified anvils with a recess (Schmidt and Rickers 2003; Manning et al. 2008; Borchert et al. 2009, 2010a, b). For the former, by using transmission geometry (Figure 1C), Sanchez-Valle et al. (2003) obtained Sr concentrations in aqueous fluids coexisting with $SrCO_3$ crystals under HTHP conditions, and Bureau et al. (2007) analyzed both melts and fluids under HTHP conditions and reported the first *in situ* partition coefficients of Pb between haplogranite melts and aqueous fluids with and without Cl. For the latter, the recess in the diamond anvil is filled with aqueous fluid, and XRF spectra of the fluid are obtained by using the 90° scattering angle geometry between the incident X-ray and detector. Borchert et al. (2009) determined concentrations of Rb and Sr in aqueous fluids coexisting with haplogranite melts under HTHP conditions, and they also analyzed quenched glasses to calculate the partition coefficients between them. Borchert et al. (2010b) determined concentrations of Ba, La, Yb, and Y in aqueous fluids, employing similar methods but with higher excitation energy. In this study, we conducted *in situ* experiments using experimental procedures similar to those by Bureau et al. (2007) at Synchrotron SOLEIL, France.

Partition coefficients of Pb between melts and aqueous fluids ($D_{\mathrm{Pb}}^{\mathrm{fluid/melt}} = C_{\mathrm{fluid}}/C_{\mathrm{melt}}$, where C represents the weight fraction of Pb in fluid and melt) have been determined both by a quench experiment (Keppler 1996) and *in situ* observation (Bureau et al. 2007). There remains, however, a contradiction with respect to the effect of Cl ions between these two experiments; $D_{\mathrm{Pb}}^{\mathrm{fluid/melt}}$ in a Cl-bearing system was larger than in a Cl-free system using andesite melts at 0.3 GPa in the quench experiment (Keppler 1996), although an opposite result was obtained using haplogranite melts at 0.3 to 1.2 GPa, Pb being in favor to the silicate melt in the *in situ* experiment (Bureau et al. 2003, 2007). Studies using melt inclusions and submarine glasses have reported that arc basalts contain larger amounts of Cl and higher ratios of Cl/H_2O than mid-oceanic ridge basalts (MORB), which suggests that slab-derived aqueous fluids seem to bring Cl to melting regions (Stolper and Newman 1994; Roggensack et al. 1997; Kent et al. 2002; Wallace 2005; Métrich and Wallace 2008). Wallace (2005) and Métrich and Wallace (2008) compiled data sets showing a wide range of Cl/H_2O at

salinities of 1 to 15 wt.% NaCl. A recent finding of saline fluids from sub-arc mantle peridotite indicates that aqueous fluids in mantle wedge can contain 5 wt.% NaCl (Kawamoto et al. 2013). It is, therefore, important to determine the effect of Cl on the trace element partitioning between fluids and melts. In the present paper, we report *in situ* partition coefficients of Pb, Rb, and Sr between aqueous fluids and haplogranite or jadeite melts under HTHP conditions. We also show the effects of pressure and salinity on the partition coefficients to elucidate the discrepancy between the previous studies.

Methods

Starting materials in this study were Pb-, Sr-, and Rb-bearing glasses (0.7 wt.% for each element) of haplogranite (HGR) and approximately jadeite (Jd) compositions (Table 1). The glasses were prepared by melting reagent grade powders of oxides, carbonates, and a hydroxide (RbOH) at 1 atm and 1,400°C for an hour, following conventional methods described by Schairer (1950) and Schairer and Bowen (1956). Compositions of haplogranite and jadeite glasses were slightly different from initial mixtures of $Ab_{35}Or_{35}Qz_{30}$ and $NaAlSi_2O_6$, respectively, both of which had an alumina saturation index (ASI) of 1.1 (Table 1). Major element compositions of glasses were measured using an Oxford Instruments LINK ISIS energy dispersive X-ray spectrometer (EDS; Oxford Instruments, Abingdon, UK) attached to a JEOL JSM-5310 scanning electron microscope (SEM; JEOL Ltd., Tokyo, Japan) housed at the Institute of Geothermal Sciences at Beppu, Kyoto University, Japan. The analyzed areas were over 15×20 μm^2, the Faraday cup current was 0.5 nA, and the analysis time was 200 s. A ZAF correction (taking into account the interaction of the matrix with atomic number *Z*, the correction adjusts for the effect of inner absorption *A* and fluorescence) was applied.

Pieces of HGR or Jd glass were loaded with Milli-Q water (H_2O, Millipore Co., Billerica, MA, USA) or saline solutions (2.5 M NaCl + 2.5 M KCl/kg water, equivalent to 25.0 wt.% (Na, K)Cl; 2.5 M NaCl/kg water, equivalent to 12.7 wt.% NaCl; and 5 M NaCl/kg water, equivalent to 22.6 wt.% NaCl) into a rhenium gasket hole in the Bassett-type HDAC. We used diamond anvils with 1.5-mm thicknesses and 1-mm culet diameters. Thicknesses of Re gaskets before experiments were about 0.125 mm; thicknesses after experiments were not measured. Gasket hole diameters used as sample rooms were between 0.4 and 0.5 mm.

Synchrotron XRF analyses were conducted at the DiffAbs beamline at Synchrotron SOLEIL. An achromatic optical setup system using Kirkpatrick-Baez focusing mirrors was used to obtain a beam size of 9×13 μm at the full width at half maximum (FWHM). The beam intensity was estimated at about 10^9 photons/s. The incident X-ray energy for all the measurements was 17.5 keV. The sample environmental setup was similar to that used by Bureau et al. (2010). A sample in the diamond anvil cell was placed at the focal point of the microbeam. The incident angle of the X-ray beam was set to 10° with respect to the sample at the center of the diamond anvil cell. The XRF spectra were obtained in transmission geometry using a Si drift detector (SDD). An angle of 20° was imposed between the incident X-ray beam and the SDD (Figure 1C).

Sample temperature was read by two K-type thermocouples that were attached to the upper and lower diamond anvils. The thermocouple temperature was calibrated against the melting temperatures of $NaNO_3$, CsCl, and NaCl. The density of the aqueous fluids loaded into the HDAC was calculated using equations for H_2O (Haar et al. 1984) or saline solutions (Zhang and Frantz 1987), which were based on the homogenization temperature between air bubbles and fluid during cooling after the XRF measurements for each experiment. The pressure at high temperature was calculated based on those equations for the state of the solutions. We flushed 5% H_2-95% Ar gas through the diamond anvil cell during heating to prevent diamonds and cell parts from oxidation, and 25°C water was circulated around the cell to prevent the heating of cell stage, optics parts, and the detector.

X-ray fluorescence data were calibrated and checked with the measurement of a 200-μm-thick cube of NIST (National Institute of Standards and Technology) silicate glass certified reference material SRM 610 within each diamond anvil cell at ambient conditions. Recommended values for trace element abundances by Rocholl et al. (1997) were used.

We heated the sample from room temperature to the target temperature within 10 min and typically maintained the temperature for 30 to 60 min. In some experiments, we applied temperature cycles between several tens of degrees above and below the target temperature for a few minutes in order to obtain fewer and larger melt globules via thermal convection (Figure 2). We did not reach complete miscibility in any of the experiments before the analysis of fluids and melts. Heating for more than 10 min was deemed sufficient for attaining equilibrium between melts and fluids. Bureau et al. (2007) estimated the diffusivity of Pb in a haplogranitic melt at conditions of 5 wt.% H_2O at 700°C and reported that Pb atoms travel 0.05 mm/min based on the diffusivity of Pb reported by Perez and Dunn (1996). The present experimental melts had 6 wt.% H_2O or more (Table 1), which resulted in similar or higher diffusivities. Therefore, equilibrium between melt globules (<0.3 mm diameter, Figure 2) and aqueous fluids can be achieved within several minutes after reaching experimental conditions.

Table 1 Composition of starting materials, experimental conditions, and experimental summary

	Experiment name									
	HGR	**B**	**BB**	**BA**	**Jd**	**137**	**137C**	**137D**	**137E**	**137G**
Starting material		HGR	HGR	HGR		Jd	Jd	Jd	Jd	Jd
Fluid		Water	Water	5 M (Na, K)Cl		Water	2.5 M NaCl	2. 5 M NaCl	5 M NaCl	5 M NaCl
wt.% (Na, K)Cl		0	0	25.0		0	12.7	12.7	22.6	22.6
Temperature (°C)		730	730	760		770	830	830	810	820
Pressure (GPa)		0.36	1	0.84		0.47	0.32	0.43	0.62	1.29
Homogenization temperature (°C)		330	150	245		308	403	365	330	168
Fluid density (g/cm^3)		0.641	0.917	1.017		0.695	0.693	0.765	0.911	1.062
Anhydrous glass density (g/cm^3)		2.337	2.337	2.334		2.461	2.449	2.449	2.453	2.451
Weight fraction of melt H_2O		0.077	0.119	0.112		0.069	0.066	0.07	0.072	0.064
Melt density (g/cm^3)		1.941	1.973	2.038		2.095	2.097	2.122	2.188	2.261
Density ratio melt/fluid		3.029	2.151	2.005		3.013	3.024	2.775	2.402	2.13
$D_{Pb}^{fluid/melt} \pm 1\sigma$		0.065 ± 0.014	0.213 ± 0.009	2.576 ± 0.060		0.187 ± 0.026	0.593 ± 0.047	0.544 ± 0.033	1.033 ± 0.129	1.396 ± 0.133
$D_{Rb}^{fluid/melt} \pm 1\sigma$		0.039 ± 0.002	0.315 ± 0.006	1.343 ± 0.033		0.124 ± 0.007	1.450 ± 0.027	1.394 ± 0.063	1.923 ± 0.022	1.889 ± 0.099
$D_{Sr}^{fluid/melt} \pm 1\sigma$		0.021 ± 0.010	0.105 ± 0.015	0.533 ± 0.032		0.004 ± 0.001	0.029 ± 0.002	0.048 ± 0.007	0.095 ± 0.004	0.238 ± 0.009
	Starting glass	Quenched glass	Quenched glass	Not available	Starting glass	Not available	Quenched glass	Quenched glass	Quenched glass	Quenched glass
wt.% SiO_2	77.00	76.21	76.03		56.32		56.58	55.34	58.83	59.19
wt.% Al_2O_3	13.74	15.92	15.22		28.29		28.42	29.51	27.00	26.82
wt.% Na_2O	3.87	3.48	3.44		15.39		15.00	15.15	14.17	13.99
wt.% K_2O	5.39	4.39	5.31							
Raw total	98.39	86.90	87.74		99.28		87.56	90.46	84.31	84.47
ASI	1.13	1.52	1.33		1.12		1.15	1.18	1.15	1.17
CIPW norm	Qz33.9Ab32.7	Qz39.2Ab29.4	Qz35.7Ab29.1		Ab57.8Ne39.2		Ab60.0Ne36.3	Ab56.7Ne38.7	Ab68.5Ne27.8	Ab70.0Ne26.2
	Or31.9C1.5	Or26.0C5.4	Or31.4C3.8		C3.0		C3.7	C4.6	C3.7	C3.8

Qz, quartz; Ab, albite; Or, orthoclase; C, corundum; Ne, nepheline; ASI, $Al_2O_3/(Na_2O + K_2O)$ in moles. Density of aqueous fluids and pressure were calculated by equations of state of H_2O (Haar et al. 1984) or saline solutions (Zhang and Frantz 1987). H_2O concentrations in the melts were estimated by Moore et al. (1998). Anhydrous glass and hydrous melt densities were calculated by Bottinga and Weil (1970) and McBirney (1984), and Bureau and Keppler (1999), respectively. Major element compositions were recalculated to 100 total oxides. Raw total oxides were lower than 100 mainly due to H_2O abundances in quenched glasses.

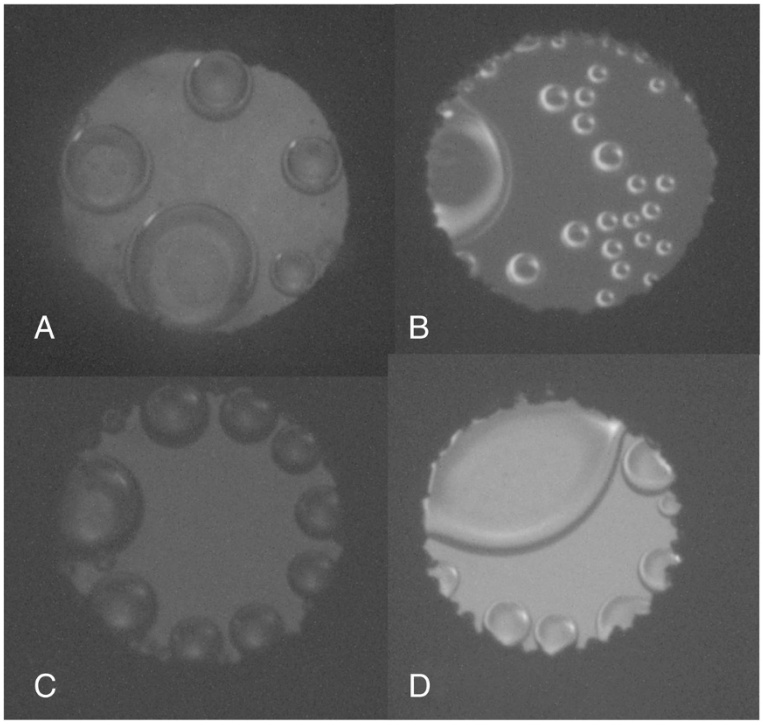

Figure 2 Transmitted light microscopic photographs. The photographs show melt globules surrounded by aqueous fluids under HTHP conditions after measurements and before quenching. The diameters of gasket holes are about 0.4 to 0.5 mm, and thickness is about 0.08 to 0.1 mm. **(A)** Exp. BB at 730°C and 1 GPa. **(B)** Exp. 137 at 770°C and 0.47 GPa. **(C)** Exp. 137E at 810°C and 0.62 GPa. **(D)** Exp. 137G at 820°C and 1.29 GPa.

Micro-XRF spectra were acquired for 300 s under HTHP conditions for several sections of the aqueous fluids and of melt globules large enough to be in contact with both of the anvil surfaces (Figures 1C and 2). The XRF peaks identified as Re L lines, Pb L lines, Rb K lines, Sr K lines, and Y K lines are shown in Figure 3. Peaks of Re can be attributed to the gasket material and peaks of Y to the ZrO_2 thermal insulator and the Si_3N_4 heater core on which the diamonds were placed (Figure 1B). The peak of the Y Kα overlapped with the peak of Rb Kβ (Figure 3).

H_2O concentrations in the haplogranite and jadeite melts were estimated for each of the pressure and temperature conditions using the empirical equation described by Moore et al. (1998). Hydrous melt densities at HTHP conditions were calculated based on melt densities of starting materials using (1) the empirical equation

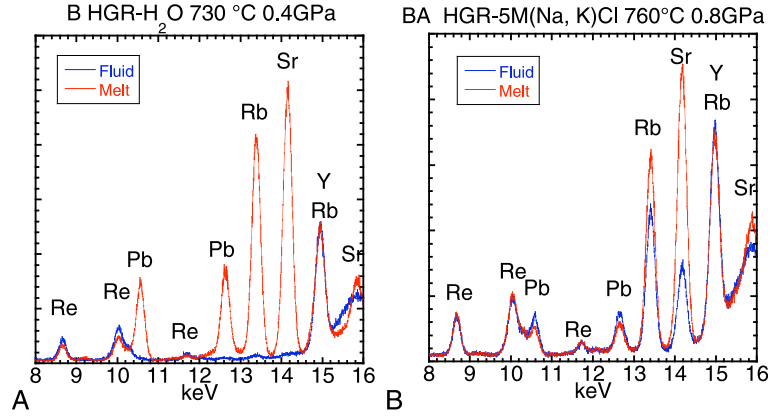

Figure 3 Representative XRF spectra of aqueous fluids and coexisting melts at HTHP conditions. Red spectra show XRF data from melt globules and blue spectra from fluids. **(A)** Exp. B at 730°C and 0.4 GPa in the haplogranite–H_2O system. **(B)** Exp. BA at 760°C and 0.8 GPa in the haplogranite–5 M (Na, K)Cl solution system.

originally suggested by Bottinga and Weil (1970) and modified by McBirney (1984), (2) the H_2O concentrations in the melts, and (3) the fluid densities (Table 1), which followed the procedures used by Bureau and Keppler (1999). Partition coefficients between fluids and melts of element i ($D_i^{\mathrm{fluid/melt}}$) were calculated using PyMCA software (Solé et al. 2007). Because we did not measure gasket thickness after each experiment, we could not calculate absolute concentrations of Pb, Rb, and Sr in melts and fluids with PyMCA. Partition coefficients were calculated by dividing the concentrations of fluid by concentrations of melt, assuming that the sample (gasket) thickness was 0.1 mm. Differences in $D_i^{\mathrm{fluid/melt}}$ values calculated for sample thicknesses of 0.08 and 0.1 mm lie within two σ. Silicate components dissolved into the fluids were ignored in the present calculations for estimating fluid densities. This assumption reduces fluid densities and increases calculated $D_i^{\mathrm{fluid/melt}}$ values. After the experiments, quenched glass samples were fixed in epoxy in the gasket and polished for the SEM-EDS analysis. The samples were quenched to glass globules, and their major element compositions were measured (Table 1).

Results

Major element compositions

Recovered samples were composed of quenched glass globules. Their chemical compositions (Table 1) were characterized by lower concentrations of Na and K and a higher concentration of Al than the starting materials, thus resulting in a higher norm corundum and higher ASI than the starting materials. This indicates that Na and K were selectively dissolved into aqueous fluids while the silicates were melted. Cl concentrations in the quenched glasses were below the detection limit (0.1 wt.%) of the EDS.

Pressure effect on partitioning

Elemental partitioning coefficients between fluids and melts ($D^{\mathrm{fluid/melt}}$) were calculated (Table 1). In order to determine the effect of pressure, partition coefficients are plotted as a function of pressure in the Cl-free water and haplogranite or jadeite systems (Figure 4A,B,C). $D_{\mathrm{Pb,\ Rb,\ Sr}}^{\mathrm{fluid/melt}}$ values obtained by the present study increase with increasing pressure (Figure 4A,B,C). The data reported by previous works are also plotted for comparison.

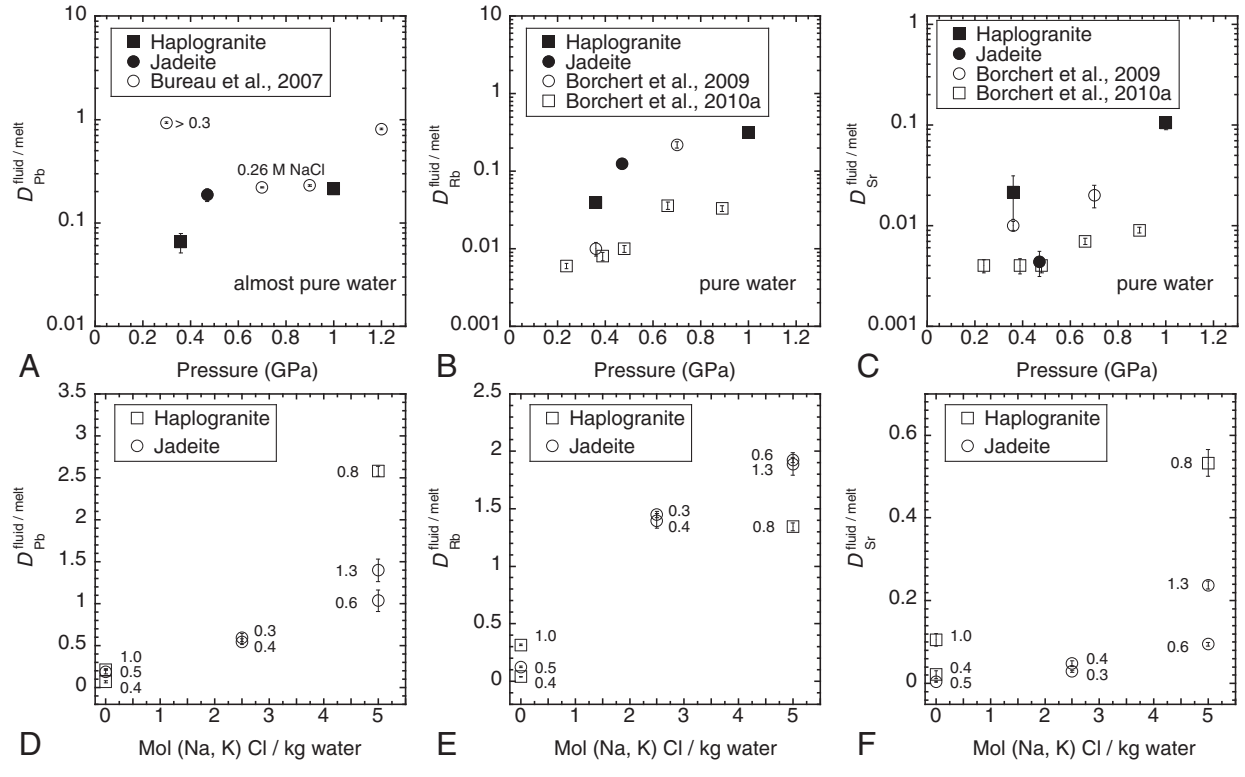

Figure 4 Partition coefficients of Pb, Rb, and Sr between aqueous fluids and coexisting haplogranite melts at HTHP conditions. (A, B, C) Partition coefficients as a function of pressure. In **(A)**, the data for $D_{\mathrm{Pb}}^{\mathrm{fluid/melt}}$ = 0.22 and 0.23 at 0.7 and 0.9 GPa, respectively, were obtained in a 0.26 M NaCl/kg water bearing system. The other data were obtained in Cl-free systems. In **(A)**, the pressure of the datum of $D_{\mathrm{Pb}}^{\mathrm{fluid/melt}}$ = 0.93 at 0.3 GPa represents the minimum pressure (Bureau et al. 2007). **(D, E, F)** Partition coefficients of Pb, Rb, and Sr as a function of NaCl + KCl in the haplogranite–H_2O system and NaCl in the jadeite–H_2O system. Numbers represent experimental pressure in GPa.

Bureau et al. (2007) reported $D_{Pb}^{fluid/melt}$ based on *in situ* analyses of haplogranite melt and aqueous fluids, and Borchert et al. (2009, 2010a) reported $D_{Rb,\ Sr}^{fluid/melt}$ based on *in situ* analysis of aqueous fluids and quenched analyses of haplogranite glasses. Two $D_{Pb}^{fluid/melt}$ data points by Bureau et al. (2007) at 0.7 and 0.9 GPa (Figure 4A) were obtained using dilute saline fluids (0.26 M NaCl/kg water), which is discussed later. Almost all $D_{Pb}^{fluid/melt}$ values increase with increasing pressure, except for one set of data plotted at 0.3 GPa and $D = 0.93$ (Bureau et al. 2007) (Figure 4A). This pressure value of 0.3 was the minimum pressure reported by Bureau et al. (2007), and the experimental pressure may actually have been higher. The other data are consistent with one another and plotted on a positive trend with pressure (Figure 4A).

$D_{Rb}^{fluid/melt}$ data reported by Borchert et al. (2009, 2010a) are plotted at a lower $D^{fluid/melt}$ for each pressure than those of the present study, except for a datum at $D = 0.22$ and 0.7 GPa (Figure 4B). $D_{Sr}^{fluid/melt}$ in the haplogranite–water is larger than that in the jadeite–water system at similar pressure (Figure 4C). The $D_{Sr}^{fluid/melt}$ data in the haplogranite–water system of the present study are larger than those by Borchert et al. (2009, 2010a) at similar pressures.

Salinity effect on partitioning

All the partition data obtained in the present study are plotted as a function of (Na, K)Cl concentrations in Figure 4D,E,F. In the jadeite–2.5 M NaCl/kg H_2O solution system (hereafter referred to as Jd-2.5 M), two D_i values for Pb, Rb, and Sr are similar to each other. Additionally, these two experiments for the same system were carried out at pressure and temperature conditions similar to each other (within ±15% relative error bar). These data attest to the reproducibility of the present experiment.

With increasing salinity in solutions, D values increase in both the haplogranite and jadeite melt systems. $D_{Pb,\ Sr}^{fluid/melt}$ values in the haplogranite system are larger than those in the jadeite system at similar pressures (Figure 4D,F). In contrast, $D_{Rb}^{fluid/melt}$ values in the haplogranite system are smaller than those in the jadeite system at similar pressures (Figure 4E). $D^{fluid/melt}$ increases as the pressure increases in the saline solution systems as well as in the Cl-free water system. Some of $D_{Pb,\ Rb}^{fluid/melt}$ values are higher than unity (Figure 4D,E). This may suggest that the present highly saline fluids and silicate melts do not approach miscibility, or they may even move away from each other, which has not been experimentally investigated. The pressure effects are not as obvious as the salinity effects for each element (Figure 4D,E,F). Cl-free aqueous fluids can transfer only one tenth (Pb, Rb) or one fifth (Sr) of elemental concentrations partitioned into the 25 wt.% (Na, K)Cl-bearing solutions (Figure 4D,E,F).

In the haplogranite–2.5 M NaCl + 2.5 M KCl/kg H_2O solution system (hereafter referred to as HGR-5 M) and jadeite–5 M NaCl/kg H_2O solution system (Jd-5 M), $D_{Pb}^{fluid/melt}$ values are larger than unity (Figure 4D), which suggests that Pb is preferentially partitioned into these saline fluids. Additionally, in Jd-2.5 or Jd-5 M and HGR-5 M, $D_{Rb}^{fluid/melt}$ values are larger than unity (Figure 4E), which suggests that Rb is preferentially partitioned into these saline fluids than coexisting melts. In summary, $D_{Pb,\ Rb,\ Sr}^{fluid/melt}$ values increase with both increasing pressure and increasing salinity.

Discussion

Partitioning behavior of Pb

The present study shows that $D_{Pb}^{fluid/melt}$ increases with increasing salinity (Figure 4D). In contrast, in the study by Bureau et al. (2007) on $D_{Pb}^{fluid/melt}$ between haplogranite (78.7 wt.% SiO_2, 12.4 wt.% Al_2O_3, 4.5 wt.% Na_2O, 4.4 wt.% K_2O) and an aqueous fluid with and without Cl, it was reported that $D_{Pb}^{fluid/melt}$ values in Cl-free fluid systems are larger than those in Cl-bearing systems (Figure 5A). Bureau et al. (2007) observed that $D_{Pb}^{fluid/melt}$ in a Cl-bearing system is about 0.2, which is smaller than the value of about 0.8 in the Cl-free system (Figure 5A). Their salinity was, however, much lower than the present study (0.26 M NaCl/kg water) and less than half of seawater (0.6 M NaCl/kg water, which is equal to 3.5 wt.%). Because the salinity of experiments carried out by Bureau et al. (2007) was much lower than that of the present study, the data plots more closely to our data in the Cl-free haplogranite system (Figure 4A), and so their $D_{Pb}^{fluid/melt}$ values can be explained by the effect of pressure in haplogranite melt in a nearly Cl-free fluid system. If this is the case, the present data and the published *in situ* data by Bureau et al. (2007) indicate that $D_{Pb}^{fluid/melt}$ increases with increasing salinity (Figures 4D and 5A). This finding is consistent with a previous study based on quench experiments at 0.3 GPa (Keppler 1996), which is discussed later.

Partitioning behavior of Rb and Sr

The present study shows that $D_{Rb,\ Sr}^{fluid/melt}$ values also increase with increasing pressure (Figure 4B,C) and salinity (Figure 4E,F) in haplogranite or jadeite melt–aqueous fluid systems. Similar characteristics of Rb and Sr were observed by Borchert et al. (2009, 2010a) in haplogranite melt–aqueous fluid systems (Figure 4B,C and Figure 5B,C). The present data in saline fluids are consistent with those reported by Borchert et al. (2009, 2010a) (Figure 5B,C). Borchert et al. (2009) stated that they did not analyze *in situ* melt droplets because of possible co-excitation of

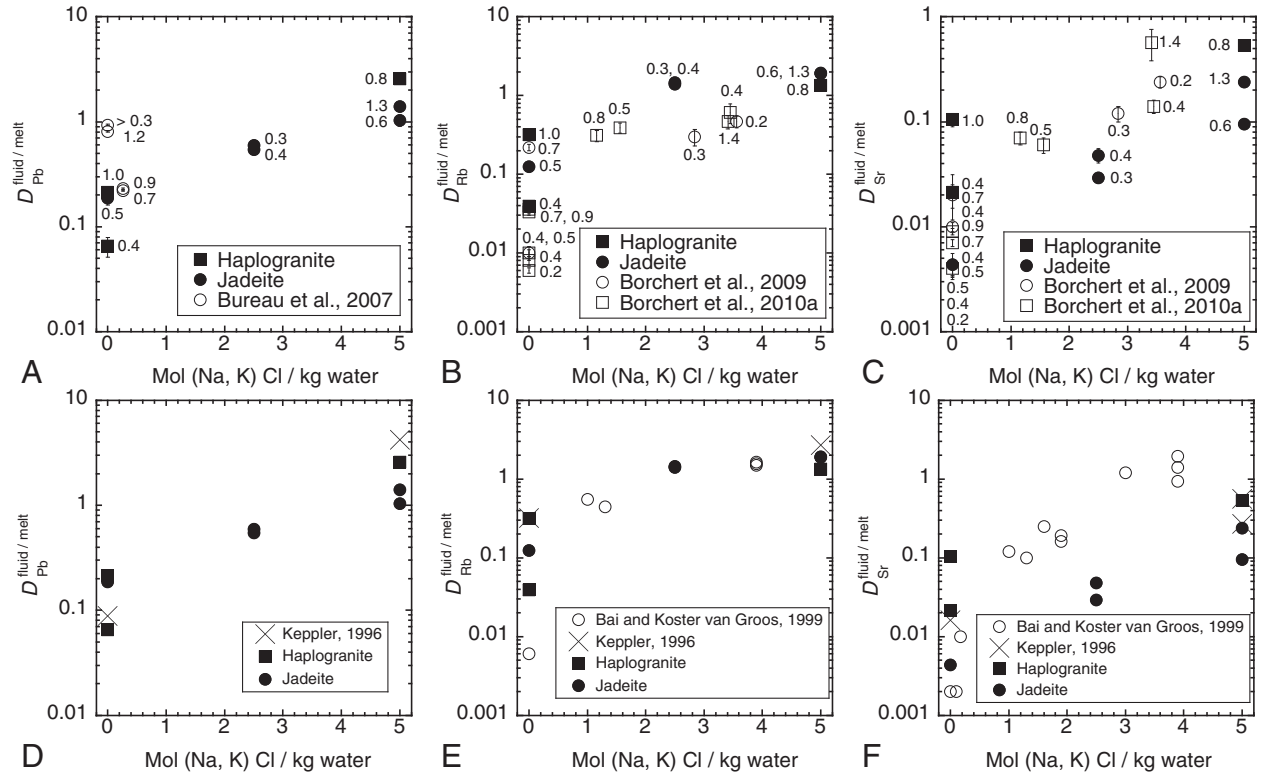

Figure 5 Comparison of the present partition coefficients with previous works. (A, B, C) Partition coefficients as a function of NaCl + KCl in haplogranite-H_2O. Comparison with previous works using *in situ* analysis (Bureau et al. 2007; Borchert et al. 2009, 2010a) is discussed in the text. Numbers represent experimental pressure in GPa. **(D, E, F)** Partition coefficients as a function of NaCl + KCl in haplogranite-H_2O. Comparison with previous works using quench experiments (Keppler 1996; Bai and Koster van Groos 1999) is discussed in the text. Experimental pressure by Keppler (1996) and by Bai and Koster van Groos (1999) is 0.3 and 0.2 GPa, respectively. The pressures in the present study are shown in **(A, B, C)**.

aqueous fluids around the droplets. If this is the case in the present experiments, the obtained XRF spectra might have been affected by the other phase and the partition coefficients might have been shifted towards unity by contamination. However, similar $D^{fluid/melt}$ values were obtained as results from two different experiments having different spatial distributions of melt globules but under similar PT conditions (Exp. 137C, 137D; see Table 1; Figure 4D,E,F at Jd-2.5 M). These data indicate that the *in situ* analyses of both melts and aqueous fluids in the present geometry (Bureau et al. 2010) have not been adversely affected, as thought by Borchert et al. (2009).

$D^{fluid/melt}$ in Cl-bearing systems are consistent with the data by Borchert et al. (2009, 2010a) (Figure 5B,C). In contrast, the present partition coefficients of Rb and Sr between haplogranite and Cl-free fluids are higher than those reported by Borchert et al. (2009, 2010a) (Figure 4B,C), with one exception ($D^{fluid/melt}_{Rb}$ = 0.22 at 0.7 GPa shown in Figure 4B; sample 5 in Table one of Borchert et al. 2009). They determined the concentrations of Rb and Sr in aqueous fluids under HTHP and analyzed those of quenched glasses. In addition to those *in situ* experiments, they also examined the effects of quenching on fluid composition by comparing their own quench experiment results with the results of *in situ* fluid analyses. They found that the partition coefficients are basically consistent in the Cl-bearing system, whereas in the Cl-free system, the $D^{fluid/melt}$ values by their quench experiments are smaller than those by their *in situ* experiments. Borchert et al. (2009, 2010a) suggest that back-reactions during quenching reduce $D^{fluid/melt}$ in the Cl-free system. In contrast, possible complexation with Cl ions prevents back-reactions in the Cl-bearing system. The discrepancy between the present study and their *in situ* and quench data in the Cl-free system can be explained by such modification by back-reactions through quenching in their experiments.

Partitioning behavior and slab-derived components

The obtained $D^{fluid/melt}$ values are consistent with those reported with quench experiments by Keppler (1996) and by Bai and Koster van Groos (1999) (Figure 5D,E,F). Keppler (1996) analyzed solutions and solutes leached by boiling with half-concentrated HCl acid for a few

minutes to dissolve the quench products from aqueous fluids. Keppler (1996) reported $D^{\text{fluid/melt}}_{\text{Pb, Rb, Sr}}$ in andesite and Cl-free water or 5 M (Na, K)Cl solution systems at 0.3 GPa and 1,040°C. Although the melt composition used in Keppler (1996) was andesite and different from haplogranite or jadeite in the present experiments, his data are consistent with the present data (Figure 5D,E,F). This consistency indicates that the experimental procedures employed by Keppler (1996) are appropriate for estimating aqueous fluid compositions in quench experiments. Bai and Koster van Groos (1999) also boiled experimental products in hot HCl acid for 10 min in order to leach solutes. Their $D^{\text{fluid/melt}}_{\text{Rb}}$ values are comparable with the present values, but their $D^{\text{fluid/melt}}_{\text{Sr}}$ values are slightly higher than the present data (Figure 5E,F). Their acid may have been too strong or their duration too long, resulting in excess Sr leaching from glasses quenched in the Cl-bearing system.

The present experiment shows that highly saline fluids can transfer Pb and Rb more effectively than Sr from the subducting oceanic lithosphere to the mantle wedge. As suggested by Keppler (1996), saline fluids can be an important agent in the transfer of large-ion lithophile elements such as Pb, Rb, and Sr in subduction zones (Perfit et al. 1980; Tatsumi and Eggins 1995). Alternatively, if the slab components are liquid-like supercritical fluids or melts (Bureau and Keppler 1999; Hermann et al. 2006; Zheng et al. 2011; Kawamoto et al. 2012), such fluids could contain large amounts of these elements even without Cl (Kessel et al. 2005b). *In situ* determination of trace element solubility in silicate-rich aqueous fluids is a feasible (Manning et al. 2008) and promising technique for understanding element transfer by fluid phases.

Geochemical studies have suggested that three components are involved in the formation of arc basalts: the depleted mantle, an aqueous fluid-like component, and a melt-like component, which are schematically illustrated in Figure 6B (Elliott et al. 1997; Pearce et al. 2005; Hanyu et al. 2012). The aqueous fluid-like and melt-like components are termed as shallow and deep subduction components, respectively (Pearce et al. 2005), and the latter is attributed to sediment-derived melts or supercritical fluids (Elliott et al. 1997; Hanyu et al. 2012). In Figure 6B, Yb is assumed not to be added from the subducting plate. In Figure 6B, concentrations of Nb, Ta, Zr, Hf, Ti, and heavy rare earth elements of the melt-like component can be underestimated as a sediment-derived melt or supercritical fluid (*cf.* Kessel et al. 2005b); however, this figure schematically shows overall characteristics of three components for sub-arc basalt chemistry. If supercritical fluids contain Cl and then subsequently separate into aqueous fluids and melts (Kawamoto et al. 2012), then it follows that such aqueous fluids will inherit much of the Cl (Borchert et al. 2010a, b) and also some of the large-ion lithophile elements. In contrast, Cl-free aqueous fluids may not be able to transfer Pb to the magma source. *In situ* characterization between aqueous fluids and melts or crystals under HTHP conditions will shed more

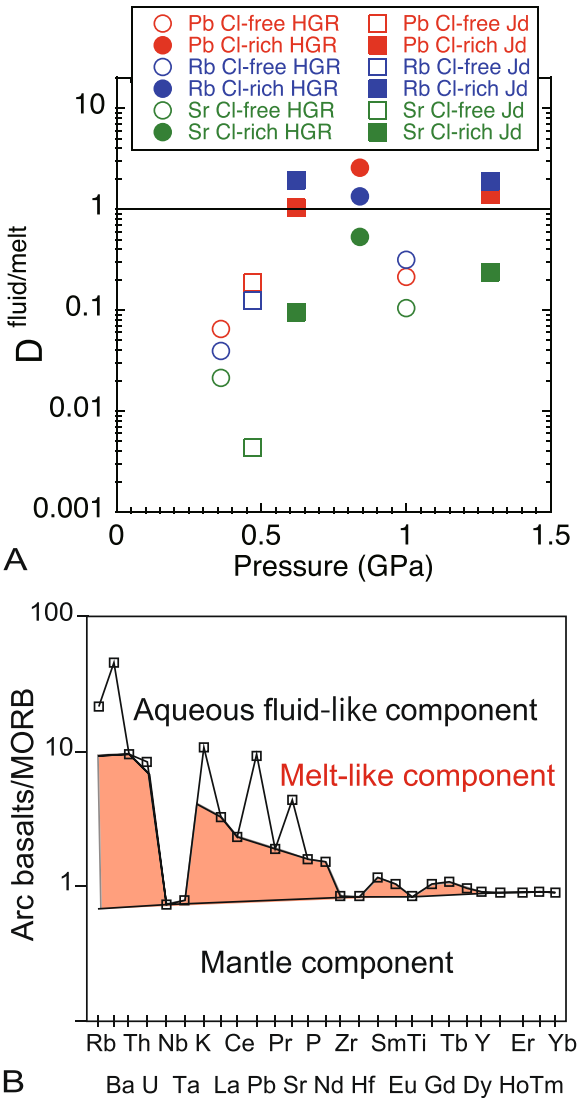

Figure 6 Experimentally determined partition coefficients ($D^{\text{fluid/melt}}_{\text{Pb, Rb, Sr}}$) and geochemical signatures of arc basalt. (A) Partition coefficients of Pb, Rb, and Sr between aqueous fluids and coexisting haplogranite (HGR) or jadeite (Jd) melts at HTHP conditions as a function of pressure. Open symbols denote data obtained in the Cl-free system, and filled symbols denote data obtained in the 5 M (Na, K)Cl/kg water system. **(B)** A schematic diagram showing the geochemical pattern for Mariana arc basalt with three components normalized by Yb. Aqueous fluid-like and melt-like components represent shallow and deep subduction components in the original Figure two (C) of Pearce et al. (2005) using the data from Elliott et al. (1997); these components are attributed to aqueous fluids and sediment-derived melt or supercritical fluids, respectively (Elliott et al. 1997; Pearce et al. 2005; Hanyu et al. 2012).

light on our quantitative understanding of the chemical composition of slab fluids including salinity and silicate components.

Conclusions

Synchrotron radiation X-ray fluorescence analysis was conducted to understand elemental partition between aqueous fluids and haplogranite or jadeite melts with Bassett-type hydrothermal diamond anvil cell at DiffAbs beamline at Synchrotron SOLEIL. A series of experiments was carried out to obtain partition coefficients of Pb, Rb, and Sr ($D^{\mathrm{fluid/melt}}_{\mathrm{Pb,\ Rb,\ Sr}}$) at 0.3 to 1.3 GPa and 730°C to 830°C under varied concentrations of (Na, K)Cl (0 to 25 wt.%). $D^{\mathrm{fluid/melt}}_{\mathrm{Pb,\ Rb,\ Sr}}$ values increase with increasing pressure and salinity. The effects of salinity and pressure on the partitioning can elucidate the discrepancy of partitioning behavior of Pb between the previous quench and *in situ* experiments (Keppler 1996; Bureau et al. 2007).

Two slab-derived components such as fluid-like and melt-like components have been suggested to explain trace element characteristics of arc basalts (Elliott et al. 1997; Pearce et al. 2005). The fluid-like component is characterized by enrichment of alkali, alkali earth elements, and Pb. These features can be explained if the fluid component is a Cl-rich aqueous fluid, because Sr and Pb are much less mobile with Cl-free fluids than Cl-rich fluids as suggested based on quench experiments (Keppler 1996). We suggest that the slab-derived components have compositional features consistent with a Cl-rich aqueous fluid and a melt, which can be formed through a separation of a slab-derived supercritical fluid (Kawamoto et al. 2012). If supercritical fluids contain Cl and subsequently separate into aqueous fluids and melts, then it follows that such aqueous fluids will inherit much of the Cl (Borchert et al. 2010a, b) and also some of the large-ion lithophile elements.

Competing interests

The authors declare that they have no competing interests.

Authors' contributions

TKa, KM, and HB designed the experiment. TKa and KM made preparations for the HTHP experiments. SR, CM, SK, DT, and HB set up the X-ray, and all authors carried out the XRF experiments at Synchrotron SOLEIL. TKa analyzed the data with the help of HB and SR, and TKa drafted the manuscript. All authors read and approved the manuscript.

Acknowledgements

The present experiment was supported by Grants-in-Aid for Scientific Research (KAKENHI) from the Ministry of Education, Culture, Sports, Science, and Technology (MEXT) and the Japan Society for the Promotion of Science (JSPS). We are grateful to the SOLEIL DIFFABS's and Surface Laboratory's staff for their constant support and availability during the synchrotron experiments. We appreciate technical assistance by Drs. Tomoyuki Shibata and Takafumi Hirata of Kyoto University and Mr. Susumu Tsujikawa of the Cyber Laser Incorporation at the initial stages of this study. Reviews by Dr. Hans Keppler of Bayeriches Geoinstitut improved the manuscript.

Author details

[1]Institute for Geothermal Sciences, Graduate School of Science, Kyoto University, Beppu 874-0903, Japan. [2]Earthquake Research Institute, The University of Tokyo, Yayoi, Tokyo 113-0032, Japan. [3]IMPMC, Sorbonne Universités, UPMC Univ Paris 06 UMR CNRS 7590 MNHN IRD, 4 Place Jussieu, Paris 75252 Paris Cedex 5, France. [4]Synchrotron SOLEIL - L'Orme des Merisiers, Saint-Aubin - BP 48, Gif-sur-Yvette 91192 Gif-sur-Yvette Cedex, France. [5]Research and Development Center for Ocean Drilling Science, Japan Agency for Marine-Earth Science and Technology, Yokosuka 237-0061, Japan. [6]Graduate School of Human and Environmental Studies, Kyoto University, Kyoto 606-8501, Japan.

Received: 19 January 2014 Accepted: 14 June 2014
Published: 27 June 2014

References

Anderson GM, Burnham CW (1965) The solubility of quartz in supercritical water. Am J Sci 263:494–511

Ayers JC, Eggler DH (1995) Partitioning of elements between silicate melt and H_2O–NaCl fluids at 1.5 and 2.0 GPa pressure: implications for mantle metasomatism. Geochim Cosmochim Acta 59:4237–4246

Bai TB, Koster van Groos AF (1999) The distribution of Na, K, Rb, Sr, Al, Ge, Cu, W, Mo, La, and Ce between granitic melts and coexisting aqueous fluids. Geochim Cosmochim Acta 63:1117–1131

Bassett WA, Shen AH, Bucknum M, Chou I-M (1993) A new diamond anvil cell for hydrothermal studies to 2.5 GPa and −190°C to 1200°C. Rev Sci Instrum 64:2340–2345

Borchert M, Wilke M, Schmidt C, Rickers K (2009) Partitioning and equilibration of Rb and Sr between silicate melts and aqueous fluids. Chem Geol 259:39–47

Borchert M, Wilke M, Schmidt C, Rickers K (2010a) Rb and Sr partitioning between haplogranitic melts and aqueous solutions. Geochim Cosmochim Acta 74:1057–1076

Borchert M, Wilke M, Schmidt C, Cauzid J, Tucoulou R (2010b) Partitioning of Ba, La, Yb and Y between haplogranitic melts and aqueous solutions: an experimental study. Chem Geol 276:225–240

Bottinga Y, Weil DF (1970) Densities of liquid silicate systems calculated from partial molar volumes of oxide components. Am J Sci 269:169–182

Brenan JM, Shaw HF, Ryerson FJ, Phinney DL (1995) Mineral-aqueous fluid partitioning of trace elements at 900°C and 2.0 GPa: constraints on the trace element chemistry of mantle and deep crustal fluids. Geochim Cosmochim Acta 59:3331–3350

Bureau H, Keppler H (1999) Complete miscibility between silicate melts and hydrous fluids in the upper mantle: experimental evidence and geochemical implications. Earth Planet Sci Lett 165:187–196

Bureau H, Ménez B, Khodja H, Daudin L, Gallien J-P, Massare D, Shaw C, Métrich N (2003) The partitioning of barium and lead between silicate melts and aqueous fluids at high pressures and temperatures. Nucl Instrum Methods Phys Res B 210:424–440

Bureau H, Menez B, Malavergne V, Somogyi A, Munoz M, Simionovici A, Massare D, Burchard M, Kubsky S, Shaw C (2005) In-situ determination of the partitioning of Pb, Rb, Sr between hydrous melts and aqueous fluids at high pressure and temperature. Geochimi Cosmochimi Acta Supp 69:A659

Bureau H, Ménez B, Malavergne V, Somogyi A, Simionovici A, Massare D, Khodja H, Daudin L, Gallien J-P, Shaw C, Bonnin-Mosbah M (2007) In situ mapping of high-pressure fluids using hydrothermal diamond anvil cells. High Pressure Res 27:1–13

Bureau H, Foy E, Raepsaet C, Somogyi A, Munsch P, Simon G, Kubsky S (2010) Bromine cycle in subduction zones through in situ Br monitoring in diamond anvil cells. Geochim Cosmochim Acta 74:3839–3850

Cullers RL, Medaris LG, Jr, Haskin LA (1970) Gadolinium: distribution between aqueous and silicate phases. Science 169:580–583

Elliott T, Plank T, Zindler A, White W, Bourdon B (1997) Element transport from slab to volcanic front at the Mariana arc. J Geophys Res 102:14991–15019

Flynn RT, Burnham CW (1978) An experimental determination of rare earth partition coeffecients between a chloride containing vapor phase and silicate melts. Geochim Cosmochim Acta 42:685–701

Green DH (1973) Experimental melting studies on a model upper mantle composition at high pressure under water-saturated and water-undersaturated conditions. Earth Planet Sci Lett 19:37–53

Haar L, Gallagher JS, Kell GS (1984) NBS/NRC steam tables. In: Thermodynamic and transport properties and computer programs for vapor and liquid states of water in SI units. Hemisphere Publishing Corp, McGraw-Hill, New York

Hanyu T, Gill J, Tatsumi Y, Kimura JI, Sato K, Chang Q, Senda R, Miyazaki T, Hirahara Y, Takahashi T, Zulkarnain I (2012) Across- and along-arc geochemical variations of lava chemistry in the Sangihe arc: various fluid and melt slab fluxes in response to slab temperature. Geochem Geophys Geosys 13. doi:10.1029/2012GC004346

Hermann J, Spandler C, Hack A, Korsakov AV (2006) Aqueous fluids and hydrous melts in high-pressure and ultra-high pressure rocks: implications for element transfer in subduction zones. Lithos 92:399–417

Kawamoto T (2006) Hydrous phases and water transport in the subducting slab. In: Keppler H, Smyth JR (ed) Water in nominally anhydrous minerals. Rev. Mineral. Geochem 62. Geochemical Society and Mineralogical Society of America, VA, USA, pp 273–289

Kawamoto T, Kanzaki M, Mibe K, Matsukage KN, Ono S (2012) Separation of supercritical slab-fluids to form aqueous fluid and melt components in subduction zone magmatism. Proc Natl Acad Sci USA 109:18695–18700

Kawamoto T, Yoshikawa M, Kumagai Y, Mirabueno MHT, Okuno M, Kobayashi T (2013) Mantle wedge infiltrated with saline fluids from dehydration and decarbonation of subducting slab. Proc Natl Acad Sci USA 110:9663–9668

Kent AJR, Peate DW, Newman S, Stolper EM, Pearce JA (2002) Chlorine in submarine glasses from the Lau Basin: seawater contamination and constraints on the composition of slab-derived fluids. Earth Planet Sci Lett 202:361–377

Keppler H, Wyllie PJ (1991) Partitioning of Cu, Sn, Mo, W, U, and Th between melt and aqueous fluid in the systems haplogranite-H_2O-HCl and haplogranite-H_2O-HF. Contrib Mineral Petrol 109:139–150

Keppler H (1994) Partitioning of phosphorus between melt and fluid in the system haplogranite-H_2O-P_2O_5. Chem Geol 117:345–353

Keppler H (1996) Constraints from partitioning experiments on the composition of subduction-zone fluids. Nature 380:237–240

Kessel R, Ulmer P, Pettke T, Schmidt MW, Thompson AB (2005a) The water-basalt system at 4 to 6 GPa: phase relations and second critical endpoint in a K-free eclogite at 700 to 1400°C. Earth Planet Sci Lett 237:873–892

Kessel R, Schmidt MW, Ulmer P, Pettke T (2005b) Trace element signature of subduction-zone fluids, melts and supercritical liquids at 120-180 km depth. Nature 437:724–727

Kushiro I (1972) Effect of water on the composition of magmas formed at high pressures. J Petrol 13:311–334

Manning CE, Wilke M, Schmidt C, Cauzid J (2008) Rutile solubility in albite–H_2O and $Na_2Si_3O_7$–H_2O at high temperatures and pressures by in-situ synchrotron radiation micro-XRF. Earth Planet Sci Lett 272:730–737

McBirney AR (1984) Igneous petrology. University Press, Oxford, p 504

Métrich N, Wallace PJ (2008) Volatile abundances in basaltic magmas and their degassing paths tracked by melt inclusions. In: Putirka K, Tepley F (ed) Minerals, inclusions and volcanic processes. Rev. Mineral. Geochem, 69. Mineralogical Society of America, VA USA, pp 363–402

Mibe K, Kanzaki M, Kawamoto T, Matsukage KN, Fei Y, Ono S (2007) Second critical endpoint in the peridotite-H_2O system. J Geophys Res 112, B03201

Moore G, Vennemann T, Carmichael ISE (1998) An empirical model for the solubility of H_2O in magmas to 3 kilobars. Am Mineral 83:36–42

Muñoz M, Bureau H, Malavergne V, Ménez B, Wilke M, Schmidt C, Simionovici A, Somogyi A, Farges F (2005) In-situ speciation of nickel in hydrous melts exposed to extreme conditions. Phys Scripta T115:921–922

Nakamura Y, Kushiro I (1974) Composition of the gas phase in Mg_2SiO_4-SiO_2-H_2O at 15 kbar. Carnegie Inst Wash Yearb 73:255–258

Pearce JA, Stern RJ, Bloomer SH, Fryer P (2005) Geochemical mapping of the Mariana arc-basin system: implications for the nature and distribution of subduction components. Geochem Geophys Geosys 6, Q07006

Perez WA, Dunn T (1996) Diffusivity of strontium, neodymium, and lead in natural rhyolite melt at 1.0 GPa. Geochim Cosmochim Acta 60:1387–1397

Perfit MR, Gust DA, Bence AE, Gust DA, Arculus RJ, Taylor SR (1980) Chemical characteristics of island-arc basalts: implications for mantle sources. Chem Geol 30:227–256

Rocholl ABE, Simon K, Jochum KP, Bruhn F, Gehann R, Kramar U, Luecke W, Molzahn M, Pernicka E, Seufert M, Spettel B, Stummeier J (1997) Chemical characterization of NIST silicate glass certified reference material SRM 610 by ICP-MS, TIMS, LIMS, SSMS, INAA. AAS and PIXE Geostandards Newslett 21:101–114

Roggensack K, Hervig RL, McKnight SB, Williams SN (1997) Explosive basaltic volcanism from Cerro Negro Volcano: influence of volatiles on eruptive style. Science 277:1639–1642

Sanchez-Valle C, Martinez I, Daniel I, Philippot P, Bohic S, Simionovici A (2003) Dissolution of strontianite at high P–T conditions: an in-situ synchrotron X-ray fluorescence study. Am Mineral 88:978–985

Schairer JF (1950) The alkali-feldspar join in the system $NaAlSiO_4$–$KAlSiO_4$–SiO_2. J Geol 58:512–517

Schairer JF, Bowen NL (1956) The system Na_2O–Al_2O_3–SiO_2. Am J Sci 254:129–195

Schmidt C, Rickers K (2003) In-situ determination of mineral solubilities in fluids using a hydrothermal diamond-anvil cell and SR-XRF: solubility of AgCl in water. Am Mineral 88:288–292

Schneider ME, Eggler DH (1986) Fluids in equilibrium with peridotite minerals: implications for mantle metasomatism. Geochim Cosmochim Acta 50:711–724

Solé A, Papillon E, Cotte M, Walter P, Susini J (2007) A multiplatform code for the analysis of energy-dispersive X-ray fluorescence spectra. Spectrochim. Acta B 62:63–68

Stolper E, Newman S (1994) The role of water in the petrogenesis of Mariana trough magmas. Earth Planet Sci Lett 121:293–325

Tatsumi Y, Eggins S (1995) Subduction zone magmatism. Blackwell Science, Cambridge, MA, USA, p 211

Wallace PJ (2005) Volatiles in subduction zone magmas: concentrations and fluxes based on melt inclusion and volcanic gas data. J Volcanol Geotherm Res 140:217–240

Zhang YG, Frantz JD (1987) Determination of homogenization temperatures and densities of supercritical fluids in the system NaCl–KCl–$CaCl_2$–H_2O using synthetic fluid inclusions. Chem Geol 64:335–350

Zheng YF, Xia QX, Chen RX, Gao XY (2011) Partial melting, fluid supercriticality and element mobility in ultrahigh-pressure metamorphic rocks during continental collision. Earth Sci Rev 107:342–374

doi:10.1186/1880-5981-66-61
Cite this article as: Kawamoto *et al.*: **Large-ion lithophile elements delivered by saline fluids to the sub-arc mantle.** *Earth, Planets and Space* 2014 **66**:61.